Adiabatic population transfer with frequency-swept laser pulses

Cite as: J. Chem. Phys. **101**, 6439 (1994); https://doi.org/10.1063/1.468368
Submitted: 21 April 1994 . Accepted: 06 July 1994 . Published Online: 31 August 1998

J. S. Melinger, Suketu R. Gandhi, A. Hariharan, D. Goswami, and W. S. Warren

Adiabatic population transfer with frequency-swept laser pulses

J. S. Melinger
Naval Research Laboratory, Code 6613, Washington, D.C. 20375 and Department of Chemistry and Princeton Center for Photonics and Opto-Electronic Materials, Princeton University, Princeton, New Jersey 08544

Suketu R. Gandhi, A. Hariharan, D. Goswami, and W. S. Warren
Department of Chemistry and Princeton Center for Photonics and Opto-Electronic Materials, Princeton University, Princeton, New Jersey 08544

(Received 21 April 1994; accepted 6 July 1994)

We present detailed experimental and theoretical results on population transfer with frequency-swept picosecond laser pulses. Here, we demonstrate that intense frequency-swept pulses, when applied in the adiabatic limit, lead to both more efficient and more selective excitation than do unmodulated laser pulses. The experimental work is performed on quasi-two-level systems (pentacene/*p*-terphenyl crystal and Na vapor), quasi-three-level systems (Na vapor), and on more complex multilevel systems (I_2 vapor). We discuss the different characteristics of adiabatic population transfer in both few-level, and multilevel cases, and, in particular, present computer calculations to explore the effects of molecular rotations in multilevel adiabatic population transfer.

I. INTRODUCTION

A prerequisite to state-to-state chemistry studies is that the "reagents" reside in a selected excited state, or set of excited states prior to the occurrence of a chemical reaction.[1] Typically, narrow-band lasers are used to populate atoms and molecules in a desired state by tuning the radiation to the resonance frequency between an initial and a target state.[2] In the limit that an ensemble of molecules consists of a set of identical two-level systems, the application of the well-known π pulse will promote 100% of the molecules from the ground state to the excited state. However, in the optical domain, inhomogeneities associated with real material transitions such as inhomogeneous broadening, Rabi frequency distribution, and multiple levels prevent any normal (unmodulated) laser pulse from acting as a π pulse for all the transitions excited by the laser bandwidth.[3] When a large degree of inhomogeneity is present, irradiation by a normal laser pulse, or from continuous wave (cw) monochromatic excitation, can transfer at best only 50% of the molecules out of the ground state to a given excited state. This may lead to ambiguity in the interpretation of experiments when, for e.g., both an initial and excited state of a reagent molecule give rise to the same product state. Therefore, there is a need to develop techniques that can transfer a greater fraction of the ensemble to a particular excited state.

In real material systems (i.e., gas phase or condensed phase), a much higher degree of population transfer may be obtained by optical excitation when the conditions for adiabatic rapid passage (ARP) are met. The application of intense frequency-swept laser pulses represents a simple method in which to achieve ARP, and may be accomplished by irradiating the material with a laser pulse whose frequency begins far below resonance, slowly sweeps through resonance, and ends with the laser frequency far above resonance (or vice versa). Enhanced population transfer by ARP has its origin in NMR spectroscopy,[4] but has also been applied in the field of optical spectroscopy.[5–12]

There has been a recent resurgence of interest in optical ARP,[8–12] which is fueled in part by the need for more selective state preparation of molecules resulting from laser excitation. On a nanosecond time scale (or longer), ARP has been achieved experimentally in a variety of ways. In one approach, molecules that possess a permanent dipole moment are Stark shifted through resonance by an applied dc electric field.[5] Here the laser frequency is kept fixed, but the transition frequency is adiabatically swept through resonance, which results in population inversion. Another approach achieves adiabatic inversion by passing a molecular beam near the focus of a cw laser beam.[7–9] Near the focus, molecules experience a linear frequency sweep because of the quadratic curvature of the phase front. This technique has been used to achieve efficient one-photon population transfer. In yet another approach, Bergmann and co-workers have utilized ARP with both cw[10(a),10(b)] and pulsed[10(c)] lasers in a counterintuitive two-photon stimulated Raman (STIRAP) configuration to selectively populate excited vibrational states in molecules with nearly 100% efficiency. In their approach ARP is achieved through proper intensity variations of the laser field (frequency sweeping is performed here), and by proper ordering of the electric field interaction sequence.

One major drawback to ARP with cw excitation of molecular beams is due to the relatively low powers available with cw lasers, which limits these applications to relatively strong molecular or atomic transitions. Another is the lack of tunable cw lasers which operate in the blue (visible) and ultraviolet portions of the spectrum. Finally, the effective pulsewidth of the cw-molecular beam method is limited by the time it takes for molecules to traverse the laser beam, which is several nanoseconds. Typically, this limits ARP applications of cw lasers to systems where the relaxation times are longer than tens of nanoseconds, however, it must be noted that the STIRAP technique remains effective even when the relaxation time of the intermediate level is shorter than the effective pulsewidth.

The most general approach to achieving adiabatic popu-

 0021-9606/94/101(8)/6439/16/$6.00

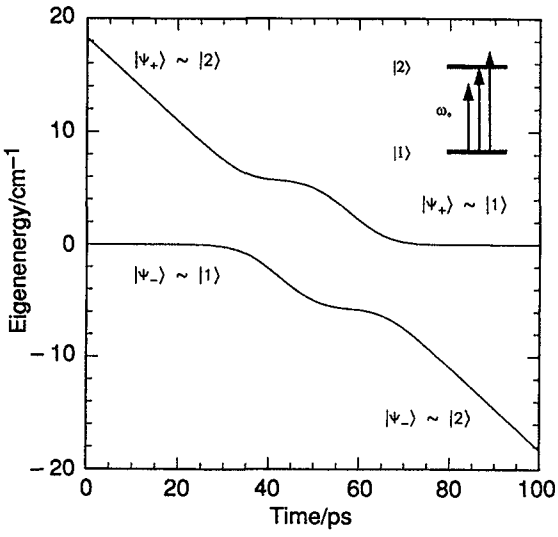

FIG. 1. Inset: two-level system irradiated by a frequency-swept laser pulse with instantaneous frequency ω_0. $|1\rangle$ and $|2\rangle$ represent the ground and excited states, respectively. The main portion of the graph shows the time evolution of the dressed energy curves for the two-level system excited by a 20 ps Gaussian pulse, $b=0.18$ cm^{-1}/ps, and $\Omega=2\pi\times10$ cm^{-1}. When the pulse frequency is well below or above resonance, the dressed eigenstates each correlate with a single "bare" state.

lation transfer is to directly modulate the frequency and amplitude of the laser pulse itself. Recently, several techniques have been demonstrated for synthesizing frequency and amplitude modulated laser pulses on the nanosecond time scale,[13] and on the picosecond and subpicosecond time scales.[14] However, for applications such as coherent population transfer, a significant improvement is obtained by modulating the laser pulse frequency alone. Specifically, simple linear optical techniques such as frequency chirping with commonly available optics[15,16] can produce useful picosecond and subpicosecond laser pulses with a moderately linear frequency sweep. In our preliminary work we demonstrated enhanced population transfer and selective excitation by ARP with frequency-swept (chirped) picosecond laser pulses.[11] Furthermore, the recent work of Broers *et al.* has used chirped ultrafast laser pulses to achieve "ladder" climbing in Rb vapor.[12]

In this paper we describe how frequency-swept picosecond laser pulses are used to achieve efficient population transfer via ARP. The remainder of this paper is organized as follows. In Sec. II we present some of the basic theoretical considerations that are useful for understanding ARP in both few-level, and multilevel systems. In Sec. III we give a detailed account of the experimental setup and techniques used to generate frequency-swept laser pulses. In Sec. IV we present results of coherent population transfer experiments on solid phase and vapor phase systems, and compare the results to theoretical calculations on model systems. Finally, in Sec. V we suggest experimental applications that will benefit from this technique.

II. THEORETICAL CONSIDERATIONS

A. Two-level systems

It is instructive to begin a discussion of the excitation properties of frequency-swept laser pulses by reviewing the results of the two-level system, as depicted in Fig. 1. The eigenkets $|1\rangle$ and $|2\rangle$ represent the ground and excited states of the zeroth-order Hamiltonian. A laser pulse with linear polarization is applied to the $|1\rangle\rightarrow|2\rangle$ transition such that the pulse frequency sweeps through resonance with the transition frequency ω_{21}. The Hamiltonian in rotating wave approximation may be written in the frequency modulation frame[4] as

$$\mathbf{H}(t)=\hbar\begin{bmatrix} 0 & \frac{\Omega(t)}{2} \\ \frac{\Omega^*(t)}{2} & \Delta(t) \end{bmatrix}. \tag{1}$$

Here, $\Delta(t)$ is the time-dependent detuning from resonance, and is written as

$$\Delta(t)=(\omega_{21}-\omega_0)+d\phi(t)/dt, \tag{2}$$

where ω_0 is the carrier frequency of the applied laser field, and $\phi(t)$ is the time-dependent phase of the laser field. The Rabi frequency is represented by $\Omega(t)$, and is written as

$$\Omega(t)=\mu\epsilon(t)/\hbar, \tag{3}$$

where $\epsilon(t)$ is the time-dependent amplitude of the applied electric field, and μ is the transition dipole moment.

ARP is often explained in the vector model.[17] In this picture, a frequency-swept laser pulse causes the pseudofield vector $\mathbf{F}$ to exert a torque on the dipole moment $\boldsymbol{\mu}$, which forces $\boldsymbol{\mu}$ to precess around $\mathbf{F}$. The vector components of $\boldsymbol{\mu}$ and $\mathbf{F}$ are just the elements of the density matrix ρ and H, respectively:

$$\mu_x=(\rho_{12}+\rho_{21})/2, \tag{4a}$$

$$\mu_y=(\rho_{12}-\rho_{21})/2i, \tag{4b}$$

$$\mu_z=(\rho_{11}-\rho_{22}), \tag{4c}$$

$$F_x=(H_{12}+H_{21})/2, \tag{5a}$$

$$F_y=(H_{12}-H_{21})/2i, \tag{5b}$$

$$F_z=(H_{11}-H_{22}). \tag{5c}$$

The application of a (red-to-blue) frequency-swept laser pulse causes the dipole moment vector to rotate from the $+z$ direction (far below resonance) to the $-z$ direction (far above resonance). When the frequency sweep is performed slowly compared to the precession of the dipole vector, but rapidly compared to the characteristic relaxation times of the system, then the dipole vector adiabatically follows the pseudofield vector, hence generating complete population inversion.

An equivalent picture discusses ARP in terms of the eigenvalues and eigenvectors of the combined matter–radiation Hamiltonian, or the so-called dressed states.[18–20] For the Hamiltonian of Eq. (1) The eigenvectors are

$$|\Psi_-(t)\rangle = \cos[\Theta(t)/2]|1\rangle - \sin[\Theta(t)/2]|2\rangle, \quad (6a)$$

$$|\Psi_+(t)\rangle = \sin[\Theta(t)/2]|1\rangle + \cos[\Theta(t)/2]|2\rangle \quad (6b)$$

and

$$\cos[\Theta(t)] = \frac{\Delta(t)}{\sqrt{\Delta^2(t)+|\Omega(t)|^2}}, \quad (7a)$$

$$\sin[\Theta(t)] = \frac{|\Omega(t)|}{\sqrt{\Delta^2(t)+|\Omega(t)|^2}}. \quad (7b)$$

The dressed state eigenvalues (eigenfrequencies) are

$$\omega_\pm(t) = [\Delta(t) \pm \sqrt{\Delta^2(t)+|\Omega(t)|^2}]/2. \quad (8)$$

In the dressed state picture, adiabatic passage occurs when changes in the Hamiltonian occur sufficiently slowly so that the system does not change eigenstate as the Hamiltonian evolves, although the eigenstates change composition during the evolution. For a two-level system, there are two important limits that are relevant to experiments with frequency-swept laser pulses. For large positive detuning (ω_0 well below resonance), and $|\Omega(t)| \ll |\Delta(t)|$,

$$|\Psi_+(t)\rangle \to |2\rangle; \quad |\Psi_-(t)\rangle \to |1\rangle \quad (9a)$$

and

$$\omega_+(t) \to \Delta(t); \quad \omega_-(t) \to 0. \quad (9b)$$

For large negative detuning (ω_0 well above resonance) and $|\Omega(t)| \ll |\Delta(t)|$,

$$|\Psi_+(t)\rangle \to |1\rangle; \quad |\Psi_-(t)\rangle \to -|2\rangle \quad (9c)$$

and

$$\omega_+(t) \to 0; \quad \omega_-(t) \to \Delta(t). \quad (9d)$$

Referring to Fig. 1, if the system initially begins in dressed state $|\Psi_-(t)\rangle$ (large positive Δ; $|\Psi_-(t)\rangle \to |1\rangle$), and evolves only along the energy curve associated with $|\Psi_-(t)\rangle$, then complete adiabatic inversion ($|1\rangle \to |2\rangle$) occurs as the frequency sweep is completed (large negative Δ).

The general condition for ARP may be expressed as the inequality[19,20]

$$\left|\left\langle \Psi_n(t)\left|\frac{d}{dt}\Psi_m(t)\right\rangle\right| \ll |\omega_n(t)-\omega_m(t)|. \quad (10)$$

For the special case of the two-level system, this inequality reduces to

$$\left|\Delta(t)\frac{d\Omega(t)}{dt} - \Omega(t)\frac{d\Delta(t)}{dt}\right| \ll [\Delta^2(t)+\Omega^2(t)]^{3/2}. \quad (11)$$

Equation (11) illustrates that ARP requires a sufficiently slow change in both the Rabi frequency and the detuning.

We now qualitatively illustrate the characteristics of adiabatic population transfer by numerically evaluating the Liouville equation

$$d\rho(t)/dt = (1/i\hbar)[\mathbf{H}(t),\rho(t)]. \quad (12)$$

The simulations are performed using a pulse with a Gaussian intensity profile of the form

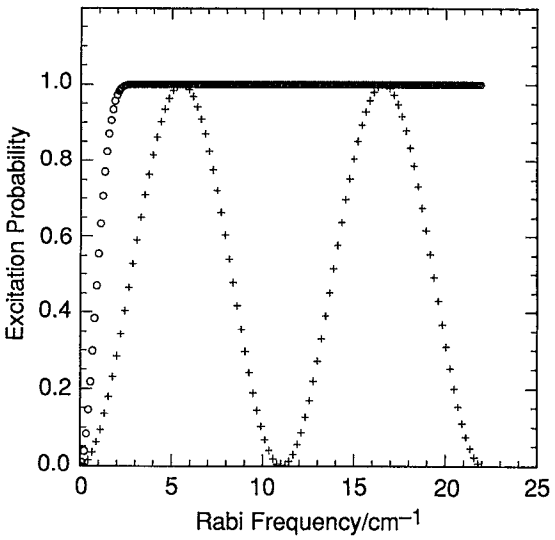

FIG. 2. Comparison of the probability of excitation as a function of applied Rabi frequency, for 2 ps transform-limited (Gaussian) pulses, indicated by crosses (+), and bandwidth equivalent 20 ps frequency-swept (Gaussian) pulses, indicated by circles (O).

$$I(t) = \exp\left(-\frac{4\ln 2t^2}{\tau_p^2}\right), \quad (13)$$

where τ_p is the FWHM of the pulse, and using a linear frequency sweep

$$\Delta(t) = 2bt, \quad (14)$$

where b is the sweep rate.

Figure 2 shows plots of the time evolution of the upper state population (ρ_{22}) as a function of applied Rabi frequency. The pulse intensity profile is either a 2 ps transform-limited pulse, or a 20 ps frequency-swept pulse of equivalent bandwidth. The familiar Rabi oscillations occur when the two-level system is excited by a transform-limited pulse. Excitation by transform-limited pulses is not robust, since the degree of inversion is sensitive to the pulse area. In contrast, in the case of excitation by a frequency-swept pulse, Rabi oscillations do not occur. Instead, the degree of excitation rises to complete inversion when the Rabi frequency becomes strong enough to satisfy the adiabatic condition. Beyond this threshold, the inversion is robust, i.e., it remains insensitive to further increases in the applied Rabi frequency. This type of robustness resulting directly from adiabatic excitation will be demonstrated in the experiments presented below.

B. Selective population transfer in three-level systems

When a broadband laser pulse is applied to a system such that the laser bandwidth overlaps two transitions, it is possible to selectively excite one transition while suppressing the other.[11(b)] This property of subpulse-bandwidth resolution is inherent to frequency-swept pulses that are applied in the limit where adiabatic passage takes place. In this sec-

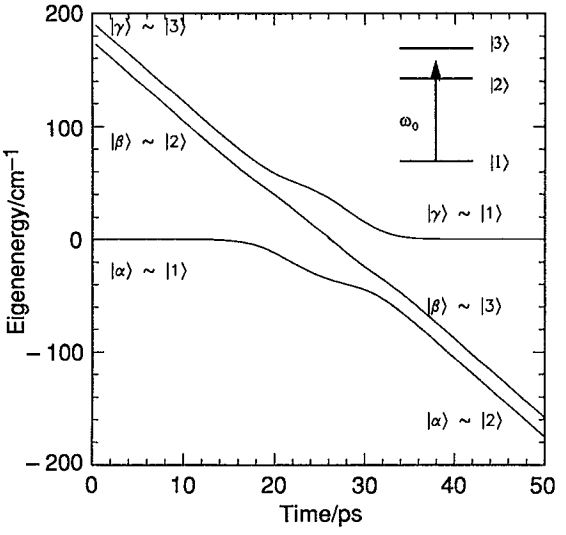

FIG. 3. Inset: three-level model for selective excitation of bare states. $|1\rangle$ represents the ground state, whereas $|2\rangle$, and $|3\rangle$ represent excited states. A broadband frequency-swept pulse is applied so that both the $1\rightarrow2$ and $1\rightarrow3$ transitions are overlapped. The main portion of the graph shows the evolution of the three eigenenergies corresponding to the dressed states $|\alpha\rangle$, $|\beta\rangle$, and $|\gamma\rangle$. A 10 ps Gaussian pulse is applied, with $b=3.5\ \mathrm{cm}^{-1}/\mathrm{ps}$, and a peak $\Omega_{12}=\Omega_{13}=2\pi\times50\ \mathrm{cm}^{-1}$. As time evolves from left to right, the pulse frequency sweeps from red to blue. A blue-to-red sweep occurs in the opposite direction. The energy separation, δ, is $2\pi\times17\ \mathrm{cm}^{-1}$.

tion we outline the mechanism for such an "adiabatic selective excitation" in terms of the three-level system shown in Fig. 3. Here a broadband pulse with a spectral bandwidth greater than the energy (frequency) separation of the upper states is applied so that its center frequency lies between the two upper states. The Hamiltonian for the transition scheme of Fig. 3 is written as

$$\mathbf{H}(t)=\hbar\begin{bmatrix} 0 & \dfrac{\Omega_{12}(t)}{2} & \dfrac{\Omega_{13}(t)}{2} \\ \dfrac{\Omega_{12}^{*}(t)}{2} & \Delta(t) & 0 \\ \dfrac{\Omega_{31}^{*}(t)}{2} & 0 & \Delta(t)+\delta \end{bmatrix}, \tag{15}$$

where $\Delta(t)=(\omega_{21}-\omega_0)+2bt$, δ is the energy (frequency) separation between $|2\rangle$ and $|3\rangle$, and $\Omega_{12}(t)$ and $\Omega_{31}(t)$ are the Rabi frequencies for the $|1\rangle\rightarrow|2\rangle$ and $|1\rangle\rightarrow|3\rangle$ transitions, respectively. The eigenvalues and eigenvectors of Eq. (15) may be obtained analytically, however, the results in this case are cumbersome. We find it more convenient to numerically evaluate the eigenvalues and eigenvectors of Eq. (15). Figure 3 shows the time evolution of the eigenvalues for excitation with a linearly swept Gaussian 10 ps laser pulse. The sweep rate b in this example is $3.5\ \mathrm{cm}^{-1}/\mathrm{ps}$, thus, the pulse spectral bandwidth (FWHM) is equivalent to that of a transform-limited 200 fs pulse. Each of the eigenvalues corresponds to an eigenvector which is labeled $|\alpha\rangle$, $|\beta\rangle$, or $|\gamma\rangle$. At early times, when the pulse frequency begins far below or above resonance, each of the eigenvectors corresponds to a single bare state, i.e.,

$$\begin{aligned} &|\alpha(t\rightarrow-\infty)\rangle\rightarrow|1\rangle; \quad |\alpha(t\rightarrow+\infty)\rangle\rightarrow|2\rangle, \\ &|\beta(t\rightarrow-\infty)\rangle\rightarrow|2\rangle; \quad |\beta(t\rightarrow+\infty)\rangle\rightarrow|3\rangle, \\ &|\gamma(t\rightarrow-\infty)\rangle\rightarrow|3\rangle; \quad |\gamma(t\rightarrow+\infty)\rangle\rightarrow|1\rangle. \end{aligned} \tag{16}$$

Figure 3 and Eq. (16) show that selective excitation of either of the upper bare states depends on both the direction of the frequency sweep (i.e., sign of b), and a strong enough Rabi frequency to satisfy the adiabatic condition of Eq. (10). For example, if the system initially begins in $|1\rangle$ at $t\rightarrow-\infty$, then an adiabatic red-to-blue frequency sweep involves evolution only along the dressed curve $|\alpha\rangle$, which results in the selective excitation of the $|1\rangle\rightarrow|2\rangle$ transition after the sweep is completed. In contrast, an adiabatic blue-to-red frequency sweep occurs along the dressed curve $|\gamma\rangle$, and selectively excites the $|1\rangle\rightarrow|3\rangle$ transition as the sweep is completed. In the results section below we present an experimental demonstration of this effect, as well as numerical calculations to model the conditions under which adiabatic selective excitation occurs.

C. Adiabatic population transfer in multilevel systems: Rotational effects

A realistic description of population transfer in molecular systems requires a more complicated level structure than the relatively simple two- and three-level systems discussed above. In general, one must consider electronic, vibrational, and rotational degrees of freedom. A number of theoretical treatments of (adiabatic) population transfer in molecules have included electronic and vibrational degrees of freedom, but they have not explored the effects of rotations.[21–28] Recently, however, Chelkowski *et al.* have discussed how rotations affect vibrational population transfer in a Morse oscillator approximation of a diatomic molecule.[26] Our preliminary experimental work on electronic population transfer in I_2 vapor indicates that rotational effects play an important role in determining the transfer efficiency.[11(a)] In this section we will explicitly include rotational levels in our theoretical model, and qualitatively discuss how they affect population transfer with frequency-swept pulses.

Our model system depicted in Fig. 4 consists of a manifold of N rotational states superimposed onto a single vibronic level in each the lower and upper electronic states. For a one-photon transition in a closed-shell diatomic the selection rule is $\Delta J=\pm1$. In this case we write the following for the nonzero matrix elements of the Hamiltonian:
For diagonal elements corresponding to the lower manifold,

$$H_{J'',J''}=B''J''(J''+1). \tag{17a}$$

For diagonal elements corresponding to the upper manifold,

$$H_{J',J'}=\hbar\Delta_{J'}(t), \tag{17b}$$

and for off-diagonal elements,

$$H_{J'',J'}=H_{J',J''}^{*}=\hbar\Omega_{J'',J'} \quad \text{for } J''=J'\pm1. \tag{17c}$$

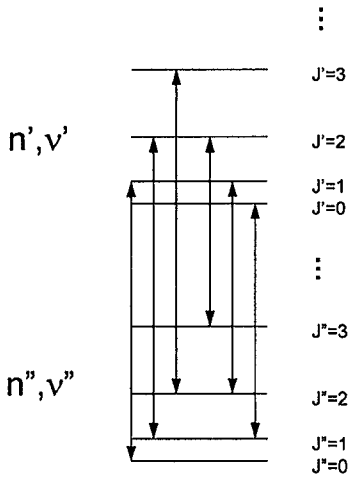

FIG. 4. Transition scheme for a model rotating diatomic molecule consisting of a manifold of rotational states superimposed upon a single upper and lower vibronic level. Here n'' and n' indicate lower and upper electronic states, and, ν'' and ν' indicate vibrational levels within each corresponding electronic state. The rotational selection rule is $\Delta J=\pm 1$.

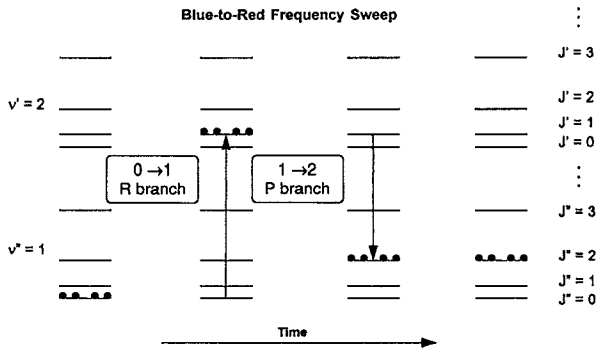

FIG. 5. Illustration of adiabatic excitation and deexcitation due to spectral overlap of both P- and R-branch transitions. In the case depicted, a blue-to-red frequency-swept pulse initially inverts the $R(0)$ transition. As the pulse frequency evolves, adiabatic excitation of the $P(1)$ transition returns population back down to the ground state manifold. The selection rules prevent further transitions back to the excited state manifold.

Here, $\Delta_{J'}(t)=[\omega_{e,g}+\omega_{\nu',\nu''}-\omega_0+B'J'(J'+1)/\hbar+2bt]$, where $\omega_{e,g}$ and $\omega_{\nu',\nu''}$ are transition frequencies for the $g\rightarrow e$ electronic transition and the $\nu''\rightarrow\nu'$ vibronic component, respectively. B'' and B' are the ground and excited state rotational constants, respectively, and $\Omega_{J'',J'}$ is the Rabi frequency for the $J''\rightarrow J'$ transition.

We distinguish among three different limits based on the width of the laser pulse spectrum ($\Delta\varpi$), with respect to the spacing of the rotational energy levels. In the first regime,

$$\Delta\varpi \ll 2B''J'',\ 2B'J'. \tag{18}$$

Here, the laser bandwidth is sufficiently narrow to resonantly excite a single ro-vibronic transition without appreciably exciting other transitions (for sufficiently small Rabi frequencies). In this limit the multilevel Hamiltonian of Eqs. (17) effectively reduces to a two-level Hamiltonian, and the dynamics of adiabatic population transfer follow that of the two-level system presented above.

In the second regime,

$$\Delta\varpi \approx 2B''J'',\ 2B'J'. \tag{19}$$

Here, the pulse bandwidth is sufficiently broad so that several different P- and/or R-branch transitions may be excited. In this regime it is impossible to ignore the effect of a broad spectral bandwidth on the two-level approximation. For example, in the case of a frequency-swept pulse, there is the possibility that molecules initially excited upward (e.g., through an upward R-branch transition) may subsequently be deexcited when the downward (P-branch) transition lies within the frequency sweep (see Fig. 5). This type of two-photon process tends to reduce the total amount of population transferred to the upper manifold. In general, to avoid deexcitation, a laser pulse should have a bandwidth less than the amount $B''(4J''+6)$ [the energy separation between the $R(J'')$ and $P(J''+2)$ transitions]. In cases where both the P- and R-branch transitions are separated ($B''\approx B'$) such deexcitation events can be avoided by confining the frequency sweep to either the P- or R-branch portions of the spectrum.

In the third regime, the laser bandwidth is significantly larger than the rotational energy level spacing,

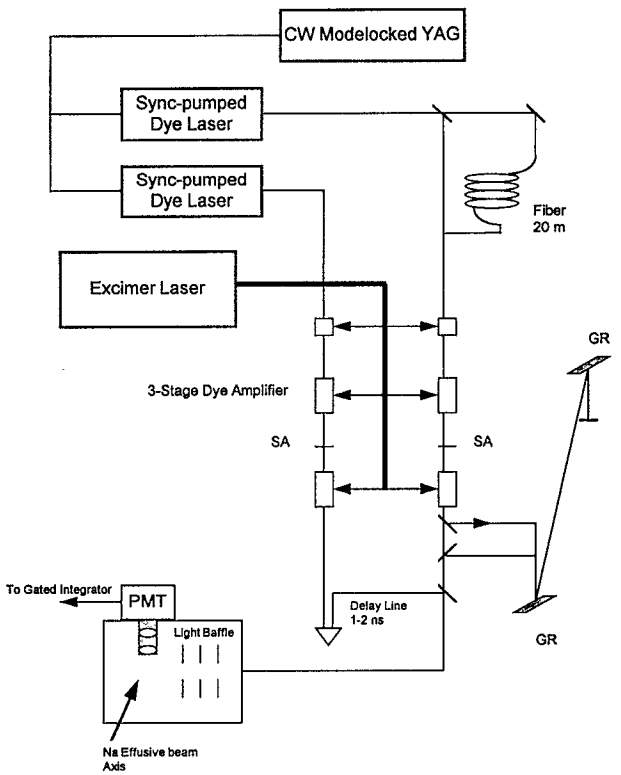

FIG. 6. Apparatus used to synthesize amplified frequency-swept picosecond laser pulses. In one method picosecond laser pulses are chirped in single mode optical fiber to create broadband pulses (before amplification). In the other method amplified pulses are chirped by double passing a diffraction grating pair. A second picosecond laser/amplifier chain produces probe pulses for detection of population transfer. SA in the amplifier chain indicates saturable absorber. Also shown is a diagram of the light collection and filtering apparatus used for the Na effusive beam experiments.

$$\Delta\varpi \gg 2B''J'',\ 2B'J'. \tag{20}$$

We discuss this regime further in Sec. IV.

III. EXPERIMENT

A. Laser system

The core of the laser apparatus consisted of a picosecond synchronously pumped dye laser system (see Fig. 6). A mode-locked frequency-doubled YAG laser (Quantronix No. 416) was configured to pump two independent tunable dye lasers. The lasers were operated with either a two or three plate birefringent filter to give nearly bandwidth-limited pulses in the range of 2–5 ps. All pulsewidths given here are derived from the FWHM of background free autocorrelation measurements.

The dye laser pulses were amplified to about 100 μJ (at 10–20 Hz) using an XeCl excimer-pumped three-stage dye cell amplifier chain. Two independent dye cell amplifiers were used for two-color experiments. A saturable absorber jet was placed between the second and third stages to limit the buildup of unwanted amplified spontaneous emission. We were careful to limit ASE to less than 5% of the final energy output. The output pulses were continuously monitored with an autocorrelator, and the wavelength measured to 0.25 cm^{-1} accuracy with a monochromator. Linearly polarized light pulses were used in all experiments.

Frequency-swept laser pulses with a nearly linear sweep were produced by either of two simple methods. In one method, laser pulses (at 76 MHz, 100 mW avg power) directly from the dye laser were coupled into 20 m of single mode fiber (4 μm core) at $\approx$60% efficiency. The combination of self-phase modulation and group velocity dispersion then broadened the laser pulse to $\approx$15 ps,[16] and produced a moderately linear red-to-blue (positive) sweep (at least over the central portion of the pulse spectrum). The laser bandwidth produced by this method exceeded 1.5 nm.

Frequency-swept pulses with a blue-to-red (negative) sweep were produced by double passing amplified laser pulses through a diffraction grating pair (1800 g/mm). The sweep rate was controlled by adjusting the separation distance of the grating pair.[15] For example, 2 ps pulses were temporally broadened to $\approx$20 ps with a grating separation of $\approx$1.5 m. The double pass, while lossy ($\approx$33% transmission), is necessary for the spatial recombination of the frequency components. Importantly, this method of temporally broadening the laser pulse does not alter the pulse spectrum.

B. Sample and detection system

Population transfer experiments were carried out on a solid state system: pentacene/*p*-terphenyl, and on gas phase systems, Na and I_2 vapor. The experiments on pentacene/*p*-terphenyl were performed at low temperature (T=3 K) using a Janis varitemp cryostat. Single mixed crystals were grown from the melt after purification by several passes of zone refining. The concentration of pentacene was kept below 5×10^{-7} mol % to avoid possible optical density effects. The sample cell containing a 1 mm thick crystal was fitted with a 1 mm circular aperture to limit excitation from the wings of the laser spot. The fluorescence detection system used to monitor population transfer was similar to that of the I_2 experiment, and is described below.

The Na experiments were carried out in a stainless steel vacuum chamber (18×18×20 in.) which was held at a nominal pressure of 10^{-6} Torr. An effusive beam of Na was generated by heating the Na metal in a stainless steel oven to ~450–550 °C, while the nozzle temperature was kept at least 50 °C above the oven temperature. The laser beam intersected the Na beam about 1 cm from the nozzle. A stainless steel baffle was placed 1–2 cm from the nozzle to confine the Na beam to the interaction region, thus limiting the optical density. Fluorescence from the Na beam was collected at 90° to the plane of the laser beam and the Na beam (cf. Fig. 6) using a pair of matched lenses. Scatter and interfering fluorescence were suppressed by spatial filtering, and by using a Schott RG-610 color filter. The signal was detected with a cooled photomultiplier tube. For the selective excitation experiments the signal was averaged by a gated integrator and stored on computer. For the SEP experiment, the transient fluorescence signal was measured with a digital oscilloscope, and then stored on computer.

The I_2 experiments were carried out in a stainless steel gas cell, as described previously.[11(a)] The sample pressure was held constant to ±5% in the range of 30–100 mTorr, and was monitored using a capacitance manometer. The diffraction grating technique was used to chirp the laser pulses, which permits an unbiased comparison of modulated and unmodulated pulses. Care was taken to ensure that the two pulses had nearly identical beam profiles as they traversed through the I_2 cell. Fluorescence from the focal region was collected at 90° using a set of spatial filters and lenses, and detected with a PMT.

IV. RESULTS AND DISCUSSION

A. Quasi-two-level systems: Pentacene/*p*-terphenyl

The simplest experimental test of adiabatic population transfer is on a material with a level structure that permits the two-level approximation for a particular set of experimental conditions. For spectral bandwidths corresponding to the picosecond regime, mixed molecular crystals at low temperature have served this role for a variety of optical coherence experiments.[29,30] In this experiment the $B_{2u}\leftarrow A_{1g}(0\text{–}0)$ transition of pentacene embedded in a *p*-terphenyl host was excited. The crystal slabs used were of good optical quality, and exhibited an inhomogeneously broadened line shape with a width (FWHM) $\approx$1.5 cm^{-1}. The fluorescence lifetime of pentacene in *p*-terphenyl is $\approx$24 ns,[30] which is much longer than any of the laser pulses used in the experiment, and ensures that we can ignore the effects of excited state relaxation.

The data shown in Fig. 7 correspond to excitation of the 0–0 line at 588.1 nm. In this example we compare the relative efficiency of population transfer for near transform-limited 3 ps laser pulses, and bandwidth equivalent 20 ps frequency-swept laser pulses chirped by the diffraction grating method. The figure can be qualitatively divided into two limiting regions (i) a low field regime (energies$\leqslant$2 μJ;

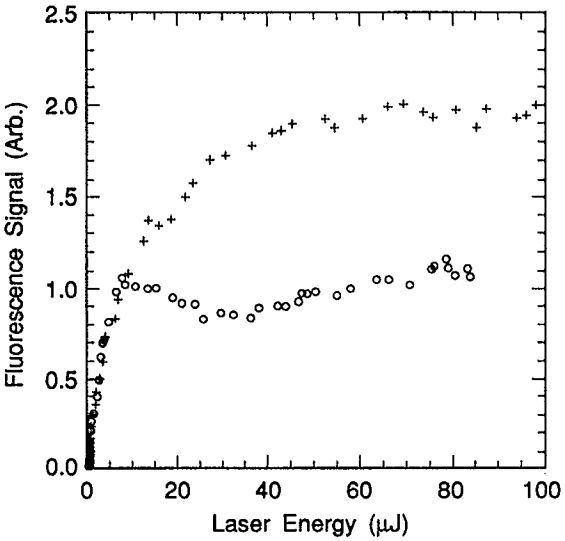

FIG. 7. Fluorescence excitation curves for the pentacene/*p*-terphenyl mixed crystal system excited by 3 ps near transform-limited laser pulses, indicated by circles (O), and by bandwidth equivalent 20 ps laser pulses chirped by the diffraction grating method, indicated by crosses (+). Each point is the average of ten laser shots. See the text for further details.

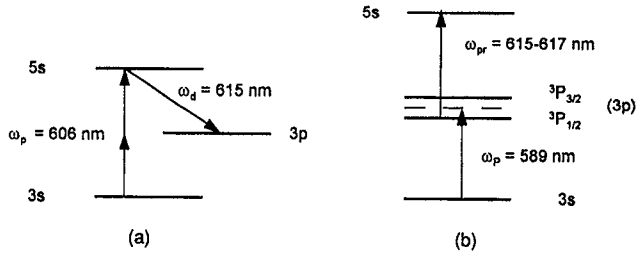

FIG. 8. (a) Experimental scheme for SEP in Na vapor. A laser "pump" pulse at 602.4 nm excites the $5s \leftarrow 3s$ transition by two-photon absorption. A subsequent "dump" pulse at 615 nm transfers population back down to the $3p$ levels. (b) Experimental scheme for selective excitation in Na vapor. A broadband frequency-swept pulse around 589 nm is tuned between the *D*-line transitions. The pulse bandwidth generated by chirping in the optical fiber (50 cm^{-1}, FWHM) is sufficient to significantly overlap both transitions, which are separated by 17 cm^{-1}. Population in either of the $3p$ levels is detected by tuning a second (unmodulated) probe pulse (3 ps, 616 nm) to a particular $5s \leftarrow 3p$ transition, and monitoring the resulting $5s \rightarrow 3p$ fluorescence.

$I_{\text{unchirped}} \leq 0.7\times10^8$ W/cm^2), and (ii) a high field regime (energies>6 μJ; $I_{\text{unchirped}} > 2\times10^8$ W/cm^2). In the low field limit the fluorescence curves from both the swept and unswept laser pulses superimpose. This is the expected result since in the low field limit (i.e., perturbative limit) the degree of excitation at frequency ω is proportional only to the pulse energy at frequency ω, hence, any frequency modulation that does not alter the pulse spectrum will have no effect. In the high field limit, there is a significant difference in the degree of fluorescence excited by frequency-swept and unswept laser pulses of equivalent bandwidth, energy, and beam profile. The fluorescence curve generated by unswept laser pulses shows a weak Rabi oscillation with maxima and minima located at ≈ 8 μJ ($I_{\text{unchirped}} \approx 2.6\times10^8$ W/cm^2), and ≈ 30 μJ ($I_{\text{unchirped}} \approx 1.0\times10^9$ W/cm^2), respectively. For comparison, if a 1 D transition dipole moment is assumed for the (0–0) $B_{2u} \leftarrow A_{1g}$ transition,[29(a)] then a 3 ps square pulse applied exactly on resonance yields maxima and minima at $I = 1.5\times10^8$ W/cm^2, and $I = 6.0\times10^8$ W/cm^2, respectively. We note that partial Rabi oscillations similar to that of Fig. 7 have been observed previously from a similar mixed crystal system.[29(a)]

The fluorescence excitation from frequency-swept laser pulses is qualitatively different. In this case there are no Rabi oscillations, but, in contrast, at the highest applied pulse energies, the amount of fluorescence excited by the frequency-swept pulses rises to nearly twice that excited by the unswept pulses. In this regime the condition for ARP is satisfied. For example, at the peak of the pulse the condition for ARP reduces to $d\Delta/dt \ll \Omega^2$. At a pulse energy of 30 μJ, $d\Delta/dt \approx 2\pi\times(4.5\times10^{21})\text{s}^{-2}$ and $\Omega^2 \approx (2\pi)^2\times(2.7\times10^{22})\text{s}^{-2}$, so that the adiabatic condition is satisfied. The observed enhancement of fluorescence from frequency-swept pulses is consistent with enhanced population transfer by ARP.

B. Quasi-two-level systems: Stimulated emission pumping

In order to quantify the degree of adiabatic population transfer in a quasi-two-level system, we performed a two-photon stimulated emission pumping (SEP) experiment in Na vapor. Figure 8(a) shows the energy level diagram for the SEP scheme used here. Initially, an unmodulated pulse at 602.4 nm excites the Na $5s \leftarrow 3s$, by two-photon absorption.[31] The population from the $5s$ state is then transferred to the $^2P_{3/2}$ level by applying a dump pulse tuned to the $5s \rightarrow {}^2P_{3/2}$ transition. The dump pulse used here was either a 3 ps near transform-limited pulse, or a bandwidth equivalent 20 ps frequency-swept pulse. The amount of population transferred back down to the $^2P_{3/2}$ level was de-

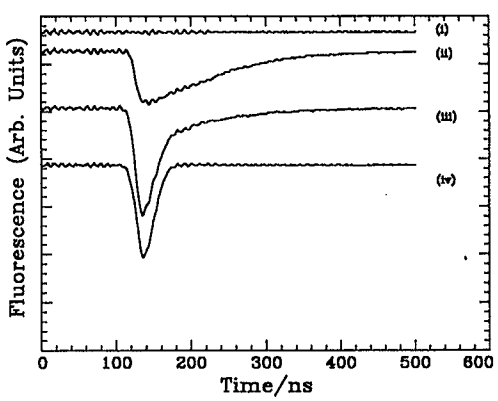

FIG. 9. Typical raw data for SEP in Na vapor. Curve (i) shows residual background scatter from the amplified laser system. Curve (ii) shows $5s \rightarrow 3p$ fluorescence excited by pump pulses alone. Curve (iii) shows typical signal that results from application of both pump and dump pulses. Here, the signal contains a strong contribution from scattered light at 616 nm. Curve (iv) shows scattered light signal from the dump pulses only.

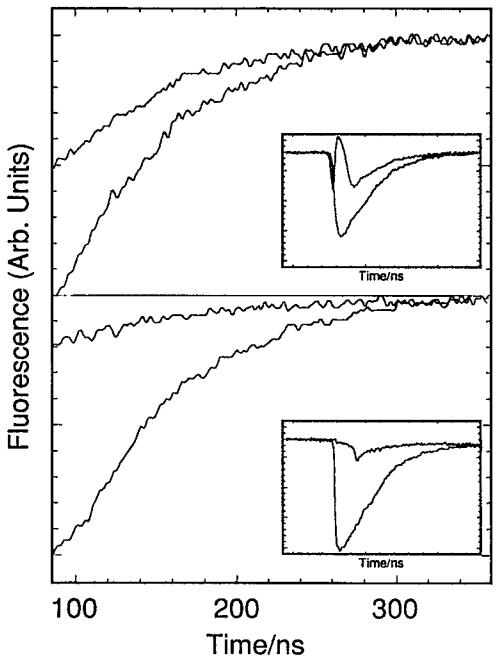

FIG. 10. SEP fluorescence decays with the background scatter, and dump pulse scatter subtracted from the "raw" signal. The upper panel illustrates how the application of unmodulated dump pulses remove only 40% of the population from the $5s$ state. Here, the lower curve represents the application of pump pulses only, and the upper curve represents the application of pump pulses followed by *unswept* dump pulses. The inset shows the full time trace. The lower panel illustrates how the application of frequency-swept dump pulses leads to 85% depletion of the population in the $5s$ state. Here, the upper curve represents the pump–dump sequence. The curves of each of the panels represents an average of 64 traces.

termined by measuring the depletion of $5s \rightarrow 3p$ fluorescence. (We note that the radiative lifetime of Na in $5s$ is $\approx$70 ns,[32] and in $3p$ is $\approx$16 ns.[33])

Figure 9 compares the raw data (shown as a negative going signal) for Na vapor excited by (i) laser pump pulses only, and (ii) laser pump pulses followed by dump pulses. In addition, we also present traces which show the interference from scattered light due to both the dump pulse and the dye amplifier. The signal in each panel represents the average of 64 fluorescence decay curves. The intense signal at early times results mainly from the residual scattered light at 615 nm from the dump pulse. The long tail in the data is mainly the $5s \rightarrow 3p$ fluorescence, with a measured time constant of $\approx$80 ns. (No attempt was made to deconvolute the instrument response time from the data.)

The "reduced data" of Fig. 10 show fluorescence decays with the scattered light subtracted. The upper panel of Fig. 10 shows the Na $5s \rightarrow 3p$ fluorescence with and without the application of the 3 ps unswept dump pulses. When the dump pulses are applied, we observe a fluorescence depletion of $\approx$40% (we compare the signal levels out in the tail to minimize the effect of any remaining component of scattered light). In contrast, the lower panel of Fig. 10 shows how frequency sweeping leads to a greater transfer efficiency. In this case a fluorescence depletion of $\approx$85% is observed. This should be compared to 100% depletion predicted in the ideal limit of ARP.

There are several experimental factors which contribute to the imperfect ($<$100%) population transfer observed in the experiment. For example, the degree of fluorescence depletion was found to be sensitive to the spatial overlap of the two pulses. This was minimized by arranging the spot size of the dump pulse to be larger than the pump pulse. Even so, since the two pulses were derived from different laser sources and traveled different optical paths, there were small differences in the spatial profiles that we did not attempt to correct. Another factor is the spatial profile of the laser beam. Na atoms which are excited in the wing of the spatial profile will not see laser fields strong enough to undergo ARP. This effect would contribute residual fluorescence from the intermediate ($5s$) state.

C. Quasi-three-level system: Selective excitation in Na vapor

The energy level diagram of Fig. 8(b) outlines the selective excitation experiment carried out in Na vapor. In this experiment a broadband chirped 15 ps pulse was recovered by injecting 3 ps pulses into an optical fiber. The pulse spectrum ($\Delta\nu \approx 50$ cm^{-1}) was sufficiently broadband to overlap both of the p levels nearly equally [see Ref. 11(b) for a typical spectrum]. To detect population transferred to either the $^2P_{3/2}$ or $^2P_{1/2}$ states, a relatively narrow band (5 ps) unmodulated probe pulse was tuned to one of the $5s \leftarrow 3p$ transitions, and the resulting fluorescence monitored.

Figure 11 shows excitation spectra for a red-to-blue sweep through the $3p \leftarrow 3s$ transitions. The excitation spectra are recorded for different positions of the center frequency of the laser spectrum (see figure caption for details). The Rabi frequencies in the figure were computed by approximating the envelope of the pulse as $\exp(-at^4)$, and using a transition dipole moment of 9 D for the $^2P_{3/2} \leftarrow {}^2S_{1/2}$ transition.[33] (In the following Ω represents the Rabi frequency for the $^2P_{3/2} \leftarrow {}^2S_{1/2}$ transition.)

The data reveal that in the low field regime (here, for $\Omega < 2\pi \times 1$ cm^{-1}) the fluorescence excitation spectrum reflects the 2:1 relative oscillator strength of the D lines. In this case, the Rabi frequency is not strong enough for ARP to occur, thus, the frequency sweep does not matter. As the applied Rabi frequency increases, the fluorescence distribution dramatically shifts. For each position of the laser center frequency the $^2P_{1/2}$ state is preferentially excited ($\approx$3:1 ratio), despite the fact that its oscillator strength is smaller by a factor of 2. These data also show a robustness of the selectivity with respect to increasing Rabi frequency, and to the position of the laser center frequency. We note here that changing the sweep direction to blue-to-red [see Ref. 11(b)] selectively excites the $^2P_{3/2}$ transition.

One of the surprising features of this experiment is that the selectivity persists even at the highest applied Rabi frequencies. Intuitively, one may expect the selectivity to degrade as the magnitude of the Rabi frequency approaches the D-line splitting ($2\pi \times 17$ cm^{-1}). This reasoning holds for excitation taking place by nearly transform-limited pulses, but, not for adiabatic excitation. To illustrate this point, density

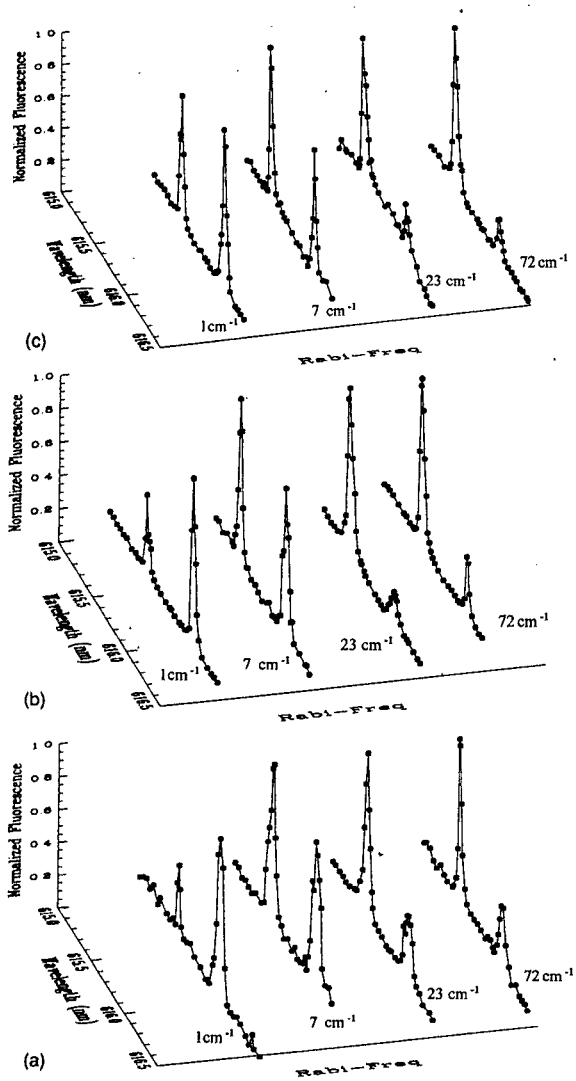

FIG. 11. Fluorescence excitation spectra showing selective excitation of the Na $3p$ levels for different choices of center frequency of the laser pulse: case (a) $\lambda_{ex}=589$ nm; case (b) $\lambda_{ex}=590$ nm (red shifted); and case (c) $\lambda_{ex}=588$ nm (blue shifted). Each data point represents the average of ten laser shots. The numbers in cm^{-1} correspond to the peak applied Rabi frequencies ($\pm 10\%$). In each of the cases the frequency sweep was from red to blue. The wavelength axis corresponds to the wavelength of the probe pulse used to transfer population from either of the $3p$ levels to the $5s$ level. The peak at 616 nm reflects population transferred to the $^2P_{3/2}$ level by the pump pulse.

matrix calculations for the Hamiltonian of Eq. (10) are presented in Fig. 12 for applied Rabi frequencies corresponding to those used in the experiment. The calculations qualitatively reproduce the experimental results for the red-to-blue sweep shown in Fig. 11. At low Rabi frequency, the calculation reproduces the 2:1 fluorescence ratio. As the Rabi frequency increases the calculation predicts the observed redistribution of fluorescence, and robustness in the applied field intensity.

Up to this point, selective excitation in Na vapor has been modeled in terms of a three-level system even though each of the D-line transitions contains splittings due to nuclear hyperfine coupling. Implicit in the three-level model is that the spectral bandwidth of the excitation pulse is far too broad to resolve the relatively small hyperfine splittings. We now examine more closely how the spectral resolution of a frequency-swept pulse is related to its pulse spectrum ($\Delta\varpi$), and its pulse duration (τ_p).

To selectively excite a single transition in a crowded spectrum with an *unmodulated* laser pulse it is necessary for the bandwidth of the pulse to be narrower than the separation between transitions, and, also, for the Rabi frequency to be sufficiently small so as not to excite off-resonant transitions. However, in the case of adiabatic excitation, both the experimental results and theoretical simulations indicate that the spectral resolution of a frequency-swept pulse may be significantly narrower than its bandwidth. Intuitively, it may be expected that for adiabatic excitation, the frequency resolution will ultimately be limited by the duration of the laser pulse τ_p. To test this assertion, density matrix calculations for the three-level system of Fig. 13 are performed for three choices of pulsewidth, each with the same sweep rate. In each simulation both the laser bandwidth and Rabi frequency exceed the 17 cm^{-1} energy separation of the p levels. We note that the longest pulse ($\tau_p=20$ ps, FWHM) has the largest spectral bandwidth, yet this pulse exhibits better selectivity than the shorter and spectrally narrower pulses. The simulation confirms that the spectral resolution of a frequency-swept laser pulse *in the strong field limit* scales with the inverse of the temporal pulsewidth. This is consistent with the uncertainty principle which limits the frequency resolution in an experiment to be no better than $1/t$—or $1/\tau_p$ in this case. The three-level approximation used above is justified in terms of the spectral width associated with the pulse width ($1/\tau_p \approx 70$ GHz) compared to the relatively small hyperfine splittings of the D lines (16–200 MHz).[34] In order to begin to resolve these splittings, the 15 ps chirped pulse used in the experiment would have to be stretched to longer than 1 ns.

D. Adiabatic population transfer in I_2 vapor

In this section we examine our experimental results on adiabatic population transfer in I_2 vapor in terms of the simple theoretical model described in Sec. II C. Some of the experimental results presented below have already been presented in an earlier communication.[11(a)]

The experiments presented here compare the efficiency of electronic population transfer in I_2 vapor for frequency-swept, and bandwidth equivalent unswept picosecond laser pulses. These pulses were used to excite the I_2 $B \leftarrow X$ transition. In contrast to the systems considered above, I_2 vapor possesses a much more complicated transition structure due to the presence of rotations. For example, in the portion of the I_2 spectrum excited here (around 600 nm) there are roughly 10–15 ro-vibronic transitions per cm^{-1},[35] hence, a 2 ps pulse will excite well over 100 different ro-vibronic transitions.

The panel shown in Fig. 14 shows I_2 $B \rightarrow X$ fluorescence excitation curves as a function of incident laser energy for different choices of laser wavelength: case I: $\lambda_{ex}=598.8$ nm; case II: $\lambda_{ex}=609.3$ nm; and case III: $\lambda_{ex}=595.9$ and 611.4 nm. In Fig. 15, for each choice of λ_{ex}, we plot a histogram

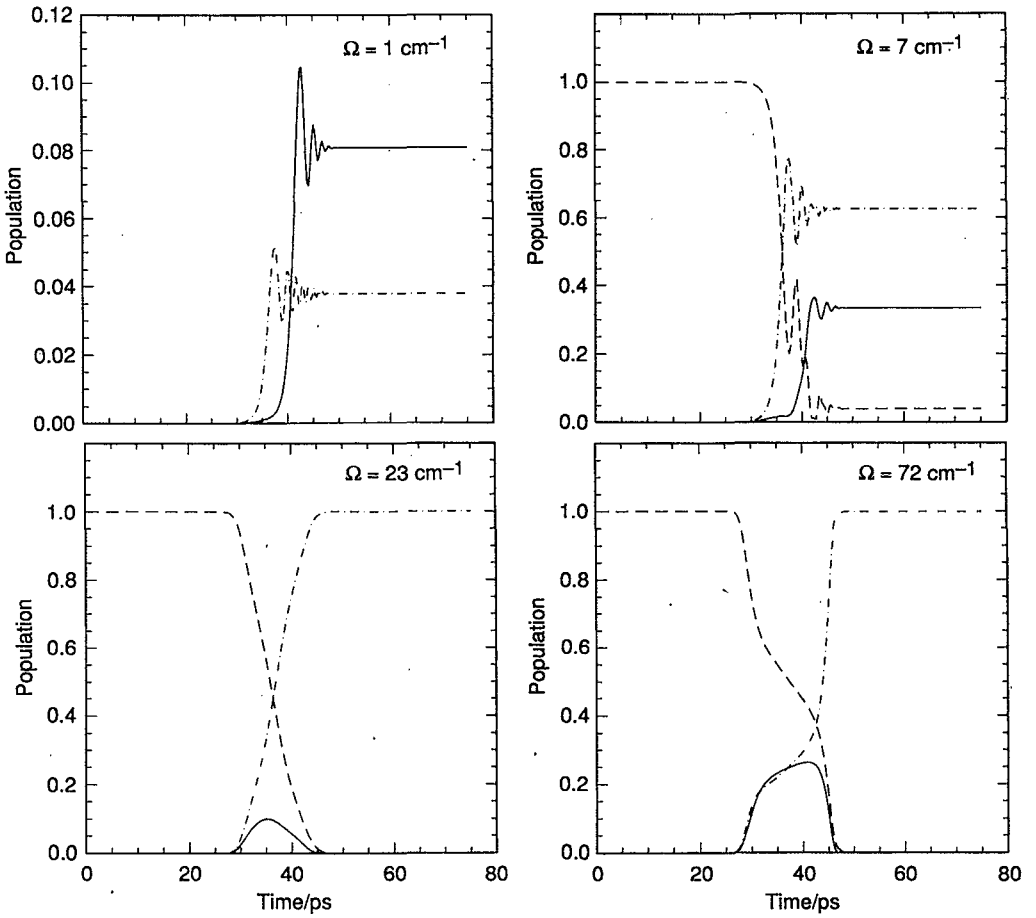

FIG. 12. Density matrix calculations using a three-level system corresponding to the Hamiltonian of Eq. (15) to model the experimental results presented in Fig. 11. The energy separation between upper levels is 17 cm^{-1}, and a pulse envelope of the form $\exp(-at^4)$ is used. The applied peak Rabi frequency in terms of the $^2P_{3/2} \leftarrow 3s$ is shown in cm^{-1}. The calculations predict the observed redistribution of fluorescence (selective population transfer) as the Rabi frequency is increased. The dashed line (---) corresponds to ρ_{11}, the dashed–dotted line (–·–) corresponds to ρ_{22} ($^2P_{1/2}$), and the solid line (—) corresponds to ρ_{33} ($^2P_{3/2}$).

showing the distribution of the ro-vibronic transitions over a 20 cm^{-1} span centered on λ_{ex}. The transition strengths for the different ro-vibronic transitions shown in the histogram depend on the particular vibrational transition excited due to the Franck–Condon overlap. The strongest transitions within these distributions have transition dipoles of ≈0.1 D.[36]

For case I, the histogram shows that the laser bandwidth overlaps ro-vibronic transitions that fall mainly in the $J''=70-140$ range. As with the previous experiments, the fluorescence excitation curve may be qualitatively divided into "low field" and "high field" regimes. For example, at applied pulse energies<15 μJ ($I_{\text{chirped}}<1.2\times10^9$ W/cm^2) the low field regime is realized, and, as expected, both swept and unswept pulses produce the same degree of fluorescence. However, as the high field regime is approached (pulse energies>15 μJ) the frequency-swept pulses begin to produce more fluorescence than do the unswept pulses of equivalent energy and bandwidth, and spot size. A pulse energy of 100 μJ produces a chirped:unchirped fluorescence ratio of ≈1.7:1, which provides evidence that in this region of the I_2 spectrum the chirped pulses are populating an increasingly large fraction of the molecules in the excited state by adiabatic inversion. For the unswept excitation, we note the absence of Rabi oscillations. This is attributed to the high degree of averaging over the large number of transitions excited (including the M_J distribution), as well as the spatial variation of the laser beam profile.

Case II represents an intermediate situation. Here, the distribution of ro-vibronic transitions is shifted somewhat towards lower J numbers with respect to case I. There is a group of transitions spanning the region $J''=60-100$ (≈65%), and group spanning the range of $J''=120-140$ (≈35%). These fluorescence excitation curves are qualitatively similar to that of case I, but with a somewhat smaller chirped:unchirped fluorescence ratio of ≈1.3:1 at 75 μJ (compare to ≈1.5:1 for case I at 75 μJ).

In contrast, case III, which was performed at $\lambda_{ex}=595.5$ and 611.4 nm, yields a qualitatively different result than cases I and II due to the different distribution of ro-vibronic transitions excited. Here, the data show that the fluorescence excited by frequency-swept and unswept pulses is nearly the same, even though the Franck–Condon factors for the tran-

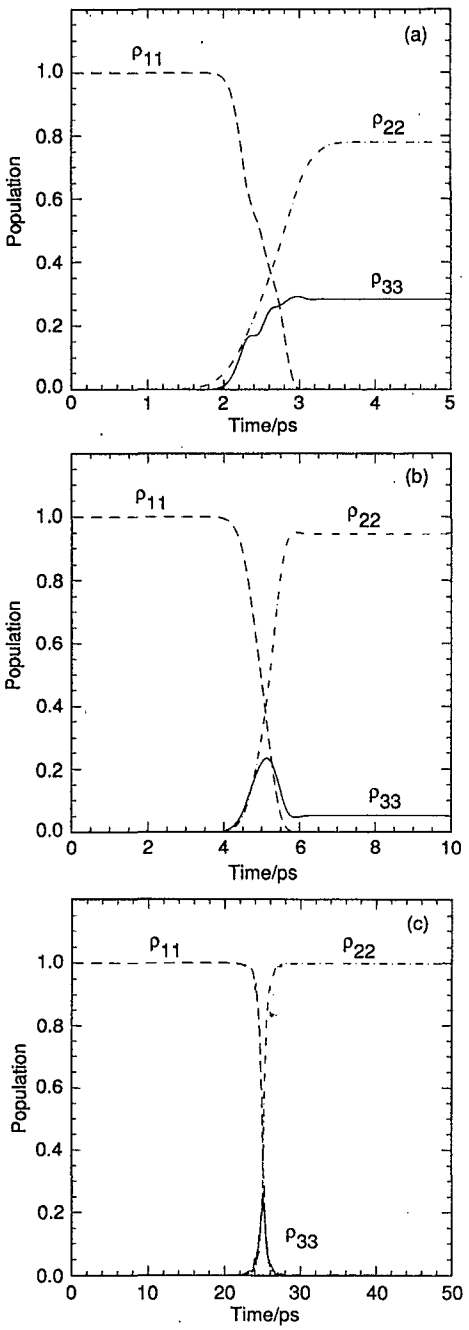

FIG. 13. Density matrix calculations showing how the degree of selectivity in a three-level system depends on the laser pulsewidth. The same energy level parameters used in the calculation of Fig. 12 are used here. Three cases are examined, each with the same sweep rate, $b=26\ \mathrm{cm}^{-1}/\mathrm{ps}$. Case (a) $\tau_p=1$ ps, case (b) $\tau_p=2$ ps, and case (c) $\tau_p=10$ ps. Gaussian amplitude profiles are used here. The panel shows that the longest pulse ($\tau_p=10$ ps) gives the best selectivity, even though this pulse possesses the largest spectral bandwidth.

sitions in this region are similar to those of cases I and II. The histograms show that low-J transitions ($J''=5$–30) account for a relatively large fraction ($\approx 75\%$) of the total transitions excited by the laser pulse, whereas the high-J transitions account for only $\approx 25\%$ of the transitions excited.

The trend shown by these experimental results is consistent with the model put forth in Sec. II C, and confirms that the high-J transitions are easier to invert than the low-J transitions. As a final check of consistency we perform density matrix calculations to simulate the fluorescence excitation curves for each choice of excitation wavelength. The calculation uses the Hamiltonian of Sec. II C [Eq. (17)] with 50 rotational levels in each of the lower and upper manifolds (100 levels overall). This number is sufficient to include the effects of off-resonant excitation. The rotational eigenfrequencies are calculated using the known rotational constants for I_2 in the X state and B state; 0.037 and 0.029 cm^{-1}, respectively.[37] In addition, the calculations include the M_J averaging of the transition moment:[38]

$$\mu(J,M_J)=\mu\sqrt{\frac{(J+1)^2-M_J^2}{(2J+3)(2J+1)}}. \tag{21}$$

Finally, the initial density matrix is given by the rotational Boltzmann distribution

$$\rho(t=-\infty)=\exp[-B''J''(J''+1)/kT]. \tag{22}$$

The results presented in Figs. 16(a)–16(c) qualitatively exhibit many of the important trends found in the experimental data. For example, in the low field regime frequency-swept and unswept pulses of equivalent energy transfer the same degree of population to the upper manifold. As the high field regime is approached, the frequency-swept pulses become more efficient for the cases shown in Figs. 16(a) and 16(b), which correspond to excitation of mainly high-J transitions. In contrast, when mainly low-J transitions are excited [Fig. 16(c)], both swept and unswept pulses show a similar degree of transfer efficiency to the upper manifold. We note here that our calculations are consistent with those performed by Chelkowski *et al.*[26] Their calculations also confirm that the high-J transitions are easier to invert than the low-J transitions.

In Figs. 16(a)–16(c) we observe that the transfer efficiency with frequency-swept pulses begins to degrade as higher Rabi frequencies are approached, and, in the case of low-J state excitation corresponding to Fig. 16(c), rather pronounced oscillations are seen. This effect is consistent with an off-resonant pumping mechanism. As the Rabi frequency continues to increase, an increasing number of off-resonant downward transitions begin to be pumped efficiently, which results in an increasing amount of population returned back to the lower manifold. To further support this explanation, Fig. 16(d) displays the transfer efficiency when the frequency sweep occurs over a smaller bandwidth (see caption for pulse characteristics). In contrast to the cases shown in Figs. 16(a)–16(c), the chirped pulse transfer efficiency continues to increase at the higher applied Rabi frequencies. Because of the smaller bandwidth, the Rabi frequency must be increased beyond $2\pi\times 7\ \mathrm{cm}^{-1}$, before deexcitation effects become significant.

Finally, we note that the calculations of Figs. 16(a)–16(c) do not reproduce the scaling of I_2 fluorescence with pulse intensity that was observed in the high field portion of fluorescence curves. There are several reasons for this. One is due to the spatial profile of the laser beam; as the pulse intensity is increased the effective focal volume also increases. Another is that as the laser intensity is increased, an

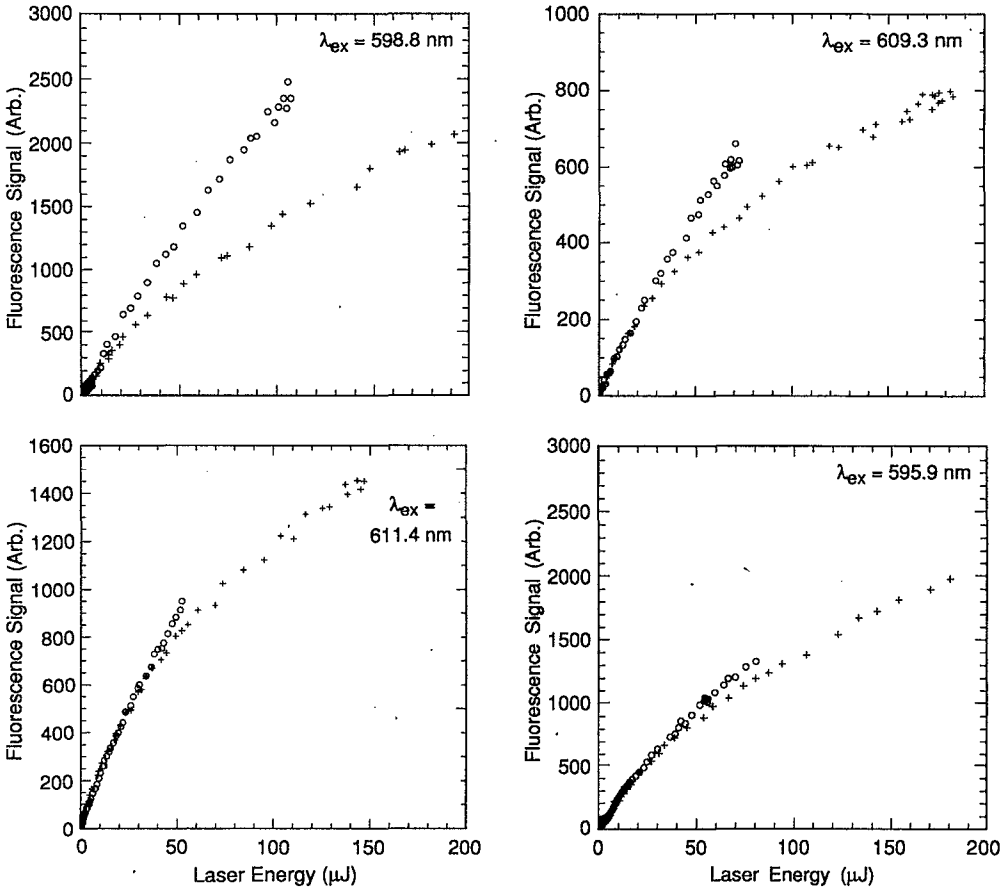

FIG. 14. I_2 fluorescence excitation curves for unchirped excitation [crosses (+)], and bandwidth equivalent chirped pulse excitation [circles (O)]. The laser spot size at the focus was ≈250 μ. The pulsewidths for unchirped and chirped pulse excitation are 2 and 20 ps, respectively. Three cases are shown which correspond to different distributions of ro-vibronic transitions: Case (I) λ_{ex}=598.8 nm, case (II) λ_{ex}=609.3 nm, and case (III) λ_{ex}=595.9 and 611.4 nm. Each data point represents the average of 20 laser shots.

increasing number of ro-vibronic states in the dense I_2 spectrum become excited. Both of these effects lead to increased fluorescence. We did not attempt to incorporate these effects into our calculations.

E. Laser bandwidth effects in a multilevel system

Up until now we have examined the dynamics of population transfer in a model rotating diatomic in the limit where the spectral bandwidth of the laser pulse is comparable to the spacings between rotational transitions. In this section we numerically examine the dynamics of population transfer in the limit that the laser bandwidth becomes much broader than the spacing between rotational transitions (the third limit in Sec. II C). Intuitively, one may expect that when the bandwidth of the excitation pulse greatly exceeds the energy level spacing, then the population transfer dynamics of the multilevel system will effectively behave as that found in a few-level (or two-level) system. In fact, we confirm this numerically for model systems where only a finite number of energy levels are important to the transition scheme. This type of model represents a realistic approximation to many atomic systems where an electronic transition is split into several components due to hyperfine interactions, and no other transitions are in near resonance. However, we illustrate below that for molecules, when the rotational structure is important, the infinite "rotational ladder" can prevent the effective collapse of a multilevel system to a two-level system.

To illustrate the effect of a broad spectral bandwidth on the dynamics of population transfer we construct a model system corresponding to a rotating diatomic with 16 rotational levels, eight in the lower energy manifold, and eight in the upper energy manifold, and with $B''=B'$. The calculations are performed for the case $M_J=0$, and the initial condition is given by the Boltzmann factor of Eq. (22). The center frequency of the laser pulse is centered on the $R(0)$ transition so that the pulse spectrum overlaps both the P- and R-branch portions of the rotational spectrum. The density matrix calculations shown in Fig. 17 illustrate qualitatively how the efficiency of population transfer to the excited state manifold changes as the rotational level spacing is decreased with respect to the bandwidth of the pulse. In each simulation the ratio B''/kT is held constant in order to preserve the

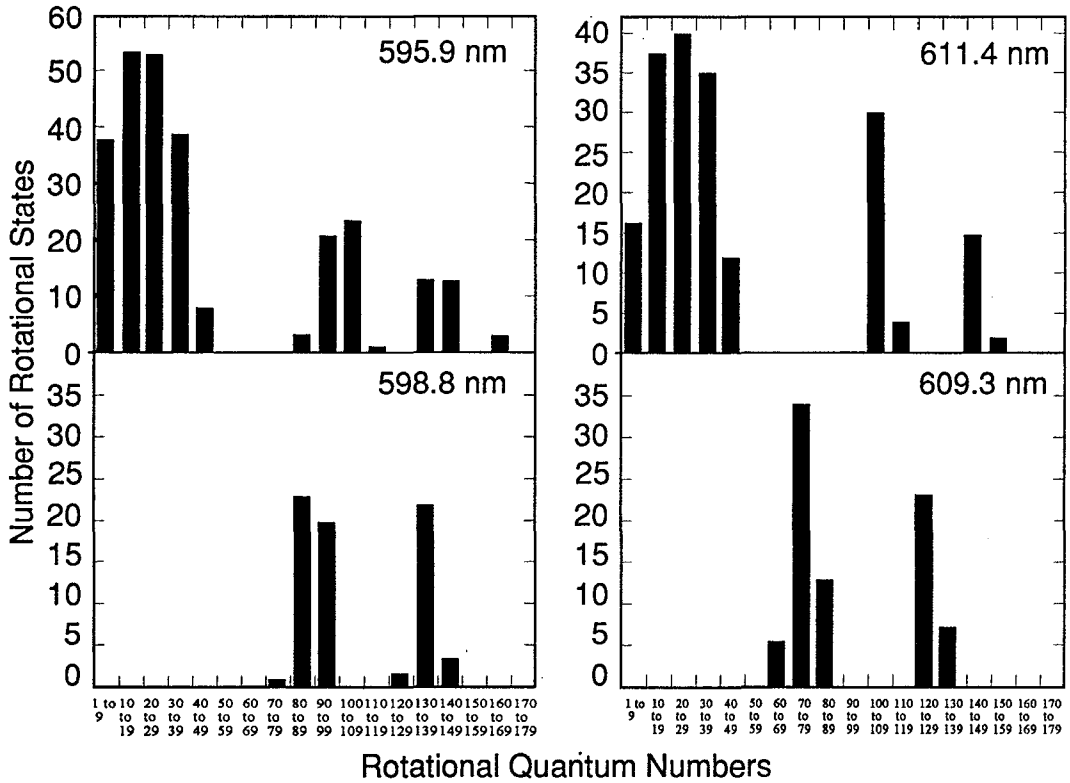

FIG. 15. Histogram plots showing the distribution of ro-vibronic transitions in I_2 vapor excited for each choice of pulse excitation wavelength in Fig. 14. The ro-vibronic transitions shown are those which overlap the pulse bandwidth over a 20 cm^{-1} span centered on λ_{ex}. The degeneracy of each transition due to the M_J quantum number is not counted here. The histograms show only the ro-vibronic transitions with line strengths within 10% of the strongest line within that spectral region.

same initial thermal distribution. Also, for each simulation, greater than 99% of the initial population resides in the $J''=0$, 1, and 2 levels. The system is driven by a 20 ps pulse with a blue-to-red frequency sweep ($\Delta\nu=7.3$ cm^{-1}, FWHM). The graphs show that as the energy level spacing becomes smaller ($B''=2.0$, 0.2, 0.02, and 0.01 cm^{-1}, respectively), the corresponding excitation curve more closely displays the characteristic two-level-type behavior, i.e., for a sufficiently strong Rabi frequency the degree of inversion to the upper manifold is complete, and remains insensitive to further changes in Rabi frequency. The calculations confirm that when the spacing between successive levels becomes sufficiently small (here for the cases $B''\leqslant 0.02$ cm^{-1}) with respect to the bandwidth of the light pulse, and when each manifold consists only of a finite number of levels, then deexcitation effects due to multiple levels are no longer important.

We now examine how the full rotational structure of a molecule, which consists of an infinite number of levels, affects the dynamics of population transfer. One important consequence of the infinite rotational ladder is that when broadband laser pulses are used, the population transfer dynamics may not simplify to that of a (quasi)-two-level system, as was illustrated above for the case that each manifold contains only a finite number of levels. This feature of population transfer dynamics is perhaps best illustrated in the dressed state picture. Figures 18(a) and 18(b) show the dressed energy curves corresponding to the case of the 16-level rotating diatomic considered above, and for $B''=0.02$ cm^{-1} [Fig. 18(a)] and $B''=0.2$ cm^{-1} [Fig. 18(b)], respectively. The Rabi frequency in each case is $2\pi\times 10$ cm^{-1}. In the former case ($B''=0.02$ cm^{-1}), the spacing between levels within each manifold is small enough so curves which originate from each the lower and upper manifolds strongly repel. Thus, population which originates in the lower manifold is transferred entirely to the upper manifold, regardless of the sweep direction. In contrast, in the latter case ($B''=0.2$ cm^{-1}), a blue-to-red frequency sweep will return a portion of the initial population back to the lower manifold because the energy curves that initially correlate (at $t=0$) to low J states ($J''=0$, 1, and 2) in the lower manifold cross with curves that correlate to high J states ($J''=7,8$) of the lower manifold as the sweep is completed ($t=100$ ps). By extrapolation, for an infinite level rotational system, there will always be a point in the eigenenergy spectrum where the type of curve crossing exhibited in Fig. 18(b) occurs, and, which prevents a complete transfer of population to the upper manifold. The point of crossing will depend on both the energy level separation (B'' and B'), and the applied Rabi frequency. We note that the curve crossing cannot be eliminated by simply applying higher Rabi frequencies, since this just shifts the crossing point to higher energy values within the eigenenergy spectrum.

Finally, for case (b) we note that reversing the sweep direction (red-to-blue) yields qualitatively different results,

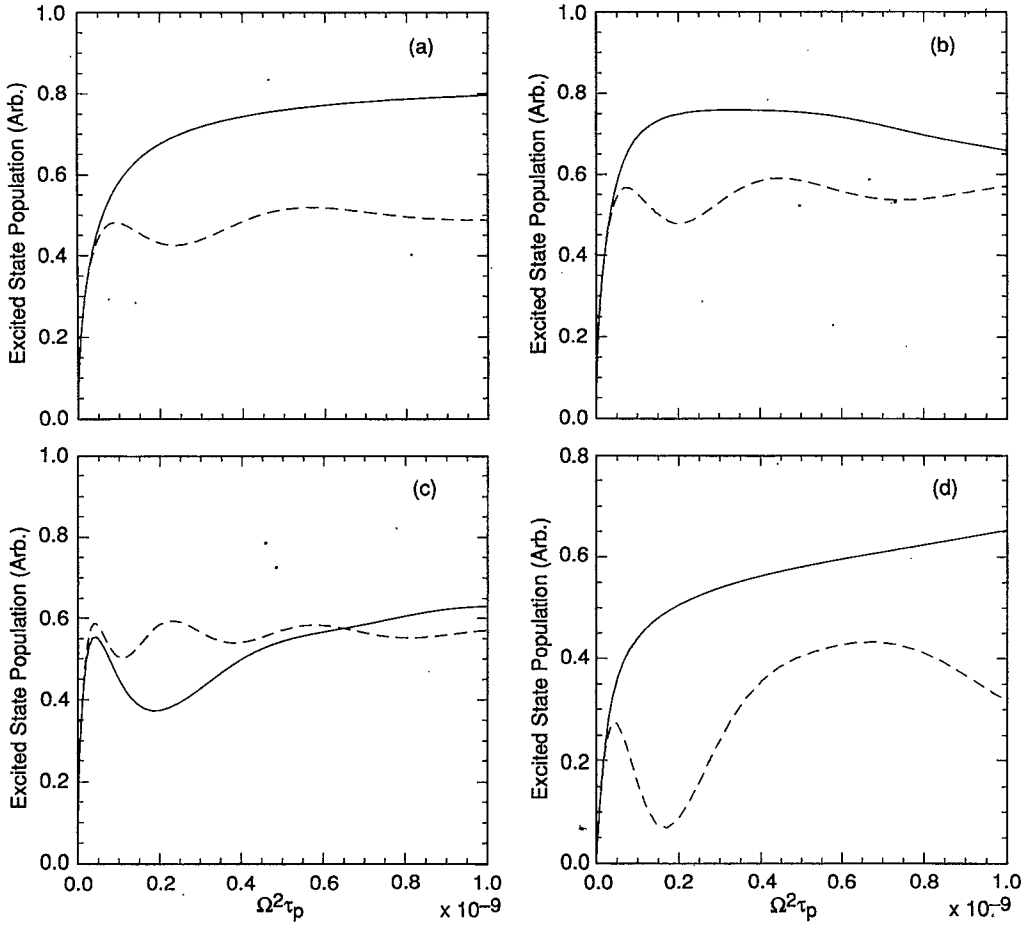

FIG. 16. Density matrix calculation to simulate experimental results for I_2. The model system includes 100 levels; 50 each in the ground state and excited state manifold. Total population in the excited manifold (sum over all upper levels) is plotted against the product of square of the Rabi frequency and the pulsewidth, τ_p {units of [(cm^{-1})^2 s]}. Here, τ_p is either 2 ps for transform-limited excitation, dashed line (---), or 20 ps for the bandwidth equivalent chirped pulse excitation (b=0.18 cm^{-1}/ps), solid line (—). The rotational eigenfrequencies are calculated using the known rotational constants for I_2 in the X state and B state; 0.037 and 0.029 cm^{-1}, respectively (Ref. 37). Three cases are shown which excite J distributions which correspond roughly to those of the three cases of Fig. 15. Case (a) ω_λ is centered at $R(100)$, case (b) ω_λ is centered at $R(60)$, and case (c) ω_λ is centered at $R(20)$. Case (d) illustrates the effect of sweeping over a smaller bandwidth. Here τ_p (transform-limited, dashed line)=2.8 ps, τ_p (bandwidth equivalent chirped pulse, solid line)=20 ps, b=0.13 cm^{-1}/ps. This calculation is performed for M_J=0, and ω_λ is centered on $R(100)$.

In this case, population which begins in the low J states of the lower manifold is adiabatically transferred to the upper manifold. For this sweep direction curves which correlate to low J states at the beginning of the sweep (t=100 ps, in this case) in the lower manifold do not cross with other curves. Here, the quasi-two-level behavior is recovered.

V. CONCLUSIONS AND FUTURE APPLICATIONS

The experimental work above has illustrated how simple experimental techniques may be used to enhance population transfer in atomic and molecular systems by ARP. In addition, we have shown how selective excitation (or suppression) of transitions overlapped by the bandwidth of the laser pulse may occur in the adiabatic limit. Enhanced population transfer to a target state by frequency sweeping works most cleanly when the material system can be approximated as a simple few-level system. In contrast, as shown in the case of I_2, multilevel effects can significantly complicate the scheme for population transfer. When multiple levels are important, the success of the simple frequency sweeping technique will depend on proper matching of the absorption spectrum of the material to the spectrum of the laser pulse.

An important quality of these experiments is their inherent insensitivity to experimental parameters (robustness). The frequency sweep of the laser pulse need not be perfectly linear, nor even monotonic; as long as the conditions for ARP are satisfied, selective excitation and enhanced population transfer will occur.

There are a variety of chemical applications which will benefit from the use of frequency-swept laser pulses. The technique, applied here to electronic population transfer, is general, so that the same principles can be applied to vibrational excitation as well. For example, frequency-swept in the infrared will be extremely useful towards the production of a highly vibrationally excited ensemble of molecules. In this application a broadband frequency swept pulse is tai-

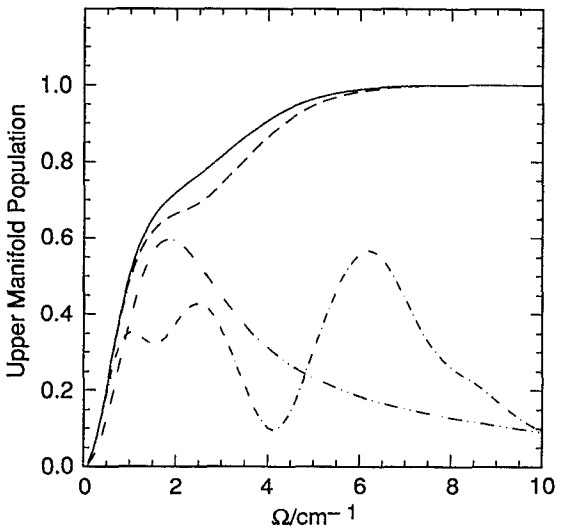

FIG. 17. Density matrix calculations for a model 16 level system (see the text for details). Each line represents the sum of individual level populations in the upper manifold. The calculations show how the dynamics of population transfer of a multilevel system begin to approximate that found in a two-level system (see, e.g., Fig. 2), as the rotational level spacing ($2B''J''$) is made smaller with respect to the pulse bandwidth. The frequency-swept pulse used here is a 20 ps Gaussian (7.3 cm^{-1}, FWHM). The value of B'' is 2.0 (–···–), 0.2 (–·–), 0.02 (---), and 0.01 cm^{-1} (—).

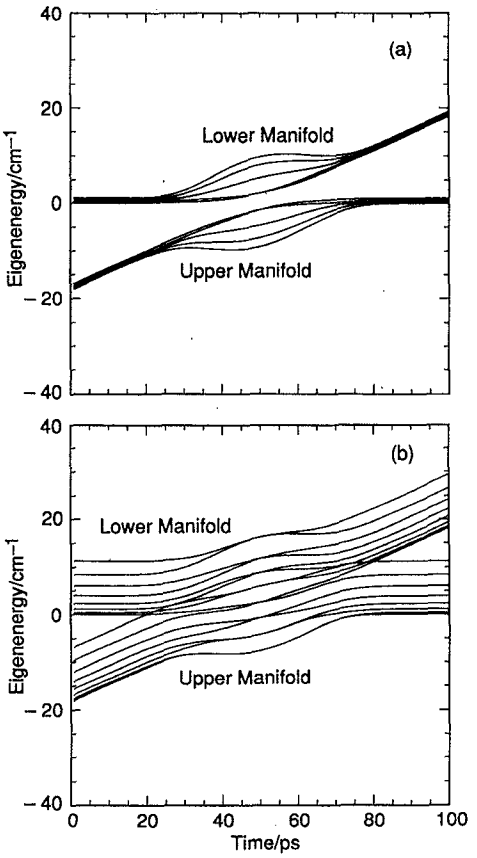

FIG. 18. Dressed energy curves for the 16-level system described in the text. Two cases are shown: (a) $B''=0.02$ cm^{-1} and (b) $B''=0.2$ cm^{-1}. The applied Rabi frequency is $2\pi \times 10$ cm^{-1} in each case. For case (a) the rotational energy level spacing is small enough compared to the Rabi frequency so that curves originating from each manifold strongly repel, thus giving rise to complete adiabatic inversion. In case (b) the separation of energy levels is larger so that curves originating from each manifold cross, giving rise to incomplete inversion for a blue-to-red sweep.

lored to successively excite vibrational transitions as it evolves. Recent theoretical work has shown how such pulses greatly enhance the production of high vibrational overtones.[21,24,26]

A more "chemistry-related" application which will benefit from efficient vibrational excitation is the study of bond-selective chemistry taking place in a bimolecular reaction. Here, a van der Waals molecule is used to restrict a reagent's geometry prior to the initiation of a reaction.[39–43] To answer a fundamentally important question: is the outcome of a bimolecular chemical reaction dependent on location of vibration energy, it is necessary to have an entire ensemble of molecules in a specific vibrational state. The experiment is depicted in Eq. (23) below. An infrared laser is used to excite a vibrational mode AB (or BC) of ABC:

$$XH\cdots ABC + h\nu_{IR} \rightarrow XH\cdots A\sim BC. \tag{23a}$$

Afterwards, molecule HX is dissociated (by a UV laser pulse). Upon dissociating of this molecule, a reaction between reagent H and ABC takes place:

$$XH\cdots A\sim BC + h\nu_{UV} \rightarrow X + H\cdots A\sim BC \rightarrow HA + BC. \tag{23b}$$

The chirped pulse technique represents an important advantage because (i) vibrational excitation can take place before the onset of vibrational predissociation (typically >100 ps[44]) and (ii) a much greater fraction of the ensemble (ideally 100%) can be transferred to a target excited vibrational state, which will reduce the contributions to products resulting from vibrationally *unexcited* molecules. Therefore, this would allow an unambiguous interpretation of the experiment.

ACKNOWLEDGMENTS

We express our gratitude to the Princeton University Chemistry Department machine shop personnel Messrs. K. Andreas, J. Vaccaro, L. Darazo, and W. Scheidt for their superb skills in the construction of the vacuum chamber used in this study. We are also grateful to Professor Klaas Bergmann (Kaiserslautern) for valuable discussions and comments regarding the subject matter of this manuscript. In addition, one of us (S.R.G.) is grateful to Mr. K. Stabe (UCLA Chemistry and Biochemistry Electronic Shop) for providing us with the sketch of the safety system for the vacuum chamber, and to Mr. Curt Hillegas, who had assisted in the construction of the alkali oven. This work was supported by the National Science Foundation under Grant No. CHE9101544, and the Office of Naval Research under Grant No. N00014-93-0533.

[1] See, for example, (a) R. B. Bernstein, *Chemical Dynamics via Molecular Beam and Laser Techniques* (Oxford University, New York, 1982); (b) R. D. Levine and R. B. Bernstein, *Molecular Reaction Dynamics and Chemical Reactivity* (Oxford University, New York, 1987).

[2] K. Bergmann, in *Atomic and Molecular Beam Methods*, edited by G.

Scoles (Oxford University, New York, 1988), Vol. 1, Chap. 12.
[3] W. S. Warren, J. L. Bates, M. A. McCoy, M. Navtratil, and L. Mueller, J. Opt. Soc. Am. B **3**, 488 (1986).
[4] W. S. Warren and M. Silver, Adv. Magn. Reson. **12**, 347 (1988).
[5] (a) M. M. T. Loy, Phys. Rev. Lett. **32**, 814 (1974); (b) **41**, 473 (1978).
[6] S. Arvillier, J. M. Raimond, Ch. J. Bordé, D. Bassi, and G. Scoles, Opt. Commun. **39**, 311 (1981).
[7] (a) A. G. Adam, T. E. Gough, N. R. Isenor, and G. Scoles, Phys. Rev. A **32**, 1451 (1985); (b) A. G. Adam, T. E. Gough, N. R. Isenor, G. Scoles, and J. Shelley, *ibid.* **34**, 480 (1986).
[8] C. Liederbaum, S. Stolte, and J. Reuss, Phys. Rep. **178**, 1 (1989).
[9] (a) V. Lorent, W. Cleays, A. Cornet, and X. Urbain, Opt. Commun. **64**, 41 (1987); (b) V. Lorent and P. Antoine, J. Phys. B **24**, 227 (1991).
[10] (a) U. Gaubatz, P. Rudecki, S. Schiemann, M. Kulz, and K. Bergmann, Chem. Phys. Lett. **149**, 463 (1988); (b) U. Gaubatz, P. Rudecki, S. Schiemann, and K. Bergmann, J. Chem. Phys. **92**, 5363 (1990); (c) S. Schiemann, A. Kuhn, S. Steverwald, and K. Bergmann, Phys. Rev. Lett. **71**, 3637 (1993).
[11] (a) J. S. Melinger, A. Hariharan, S. R. Gandhi, and W. S. Warren, J. Chem. Phys. **95**, 2210 (1991); (b) J. S. Melinger, S. R. Gandhi, A. Hariharan, J. X. Tull, and W. S. Warren, Phys. Rev. Lett. **68**, 2000 (1992); (c) J. S. Melinger, A. Hariharan, S. R. Gandhi, and W. S. Warren, in *ULTRAFAST Phenomena VIII*, edited by J.-L. Martin *et al.*, Springer Series in Chemical Physics (Springer, Berlin, 1993), Vol. 55.
[12] B. Broers, H. B. van Linden van den Heuvell, and L. C. Noordam, Phys. Rev. Lett. **69**, 2062 (1992).
[13] C. P. Lin, J. Bates, J. T. Mayer, and W. S. Warren, J. Chem. Phys. **86**, 3750 (1987).
[14] (a) J. P. Heritage, A. M. Weiner, and R. N. Thurston, Opt. Lett. **10**, 609 (1986); (b) M. Haner and W. S. Warren, *ibid.* **12**, 398 (1987).
[15] E. B. Treacy, IEEE J. Quantum Electron. **QE-5**, 454 (1969).
[16] (a) D. Grischkowsky and A. C. Balant, Appl. Phys. Lett. **41**, 1 (1982); (b) B. Nikolaus and D. Grischkowsky, *ibid.* **42**, 1 (1983).
[17] R. P. Feynman, F. L. Vernon, and R. W. Hellwarth, J. Appl. Phys. **28**, 49 (1957).
[18] (a) C. Cohen-Tannoudji and S. Haroche, J. Phys. (Paris) **30**, 125 (1969); **30**, 153 (1969); (b) P. L. Knight and P. W. Milloni, Phys. Rep. **66**, 21 (1980).
[19] See, for example, B. Shore, *Theory of Coherent Atomic Excitation* (Wiley, New York, 1990).
[20] K. Bergmann and B. W. Shore, in *Advances in Physical Chemistry*, edited by H. L. Dai and R. W. Field (World Scientific, Singapore, 1993).
[21] (a) S. Chelkowski, A. D. Bandrauk, and P. B. Corkum, Phys. Rev. Lett. **65**, 2355 (1990); (b) S. Chelkowski and A. D. Bandrauk, Chem. Phys. Lett. **186**, 264 (1991); (c) E. E. Aubanel and A. Bandrauk, J. Phys. Chem. **97**, 12620 (1993).
[22] Y. B. Band and P. S. Julienne, J. Chem. Phys. **97**, 9107 (1992).
[23] C. E. Carroll and F. T. Hioe, Phys. Rev. Lett. **68**, 3523 (1992).
[24] (a) B. Just, J. Manz, and G. K. Paramonov, Chem. Phys. Lett. **193**, 429 (1992); (b) B. Just, J. Manz, and I. Trisca, *ibid.* **193**, 423 (1992); (c) W. Jakubetz, E. Kades, and J. Manz, J. Phys. Chem. **97**, 12609 (1993); (d) J. Manz and G. K. Paramonov, *ibid.* **97**, 12,626 (1993).
[25] B. Amstrup, A. Lörincz, and S. A. Rice, J. Phys. Chem. **97**, 6175 (1993).
[26] S. Chelkowski and A. D. Bandrauk, J. Chem. Phys. **99**, 4279 (1993).
[27] G. K. Paramonov, Chem. Phys. **177**, 169 (1993).
[28] S. Ruhman and R. Kosloff, J. Opt. Soc. Am. B **7**, 1748 (1990).
[29] (a) D. E. Cooper, R. W. Olson, R. D. Wieting, and M. D. Fayer, Chem. Phys. Lett. **67**, 41 (1979); (b) D. E. Cooper, R. W. Olson, and M. D. Fayer, J. Chem. Phys. **72**, 2332 (1980); (c) T. E. Orlowski and A. H. Zewail, *ibid.* **70**, 1390 (1979).
[30] W. Hesselink and D. A. Weirsma, in *Spectroscopy and Excitation Dynamics of Condensed Molecular Systems*, edited by V. M. Agranovich and R. M. Hochstrasser (North-Holland, Amsterdam, 1983).
[31] (a) C. E. Moore, in *Atomic Energy Levels*, Natl. Bur. Stand. Circ. No. 467 (National Bureau of Standards, Washington, D.C., 1971), Vol. 1, pp. 89–91.
[32] D. Kaiser, Phys. Lett. A**51**, 375 (1975).
[33] W. L. Wiege, M. W. Smith, and B. M. Miles, *Atomic Transition Probabilities* (U.S. GPO, Washington, D.C., 1966), Vol. 2, pp. 1–7.
[34] See, for example, L. Allen and J. H. Eberly, *Optical Resonance and Two-Level Atoms* (Dover, New York, 1975).
[35] S. Gerstenkorn and P. Luc, *Atlas Du Spectre D'Absorption De La Molecule D'Iode* (CNRS, Paris, 1978).
[36] J. Tellinghuisen, J. Chem. Phys. **76**, 4736 (1982).
[37] See, for example, G. Herzberg, *Spectra of Diatomic Molecules* (Van Nostrand Reinhold, New York, 1950), pp. 540–541.
[38] C. H. Townes and A. L. Schawlow, *Microwave Spectroscopy* (McGraw-Hill, New York, 1955).
[39] C. Jouvet and B. Soep, Chem. Phys. Lett. **96**, 426 (1983).
[40] (a) K. Honma and O. Kajimoto, Chem. Phys. Lett. **117**, 123 (1985); (b) K. Honma, Y. Fujimura, O. Kajimoto, and G. Inoue, J. Chem. Phys. **88**, 4739 (1988).
[41] (a) S. Beulow, G. Radhakrishnan, J. Catanzarite, and C. Wittig, J. Chem. Phys. **83**, 444 (1985); (b) G. Radhakrishnan, S. Buelow, and C. Wittig, *ibid.* **84**, 727 (1986).
[42] N. F. Scherer, L. R. Khundkar, R. B. Bernstein, and A. H. Zewail, J. Chem. Phys. **87**, 1451 (1987).
[43] M. Takayanagi and I. Hanazaki, Chem. Rev. **91**, 1193 (1991).
[44] See, for example, F. G. Celli and K. C. Janda, Chem. Rev. **86**, 507 (1986), and references cited therein.